# Structure of Nup58/45 Suggests Flexible Nuclear Pore Diameter by Intermolecular Sliding

Ivo Melcák *et al.*

*Science* **315**, 1729 (2007);
DOI: 10.1126/science.1135730



*Science* (print ISSN 0036-8075; online ISSN 1095-9203) is published weekly, except the last week in December, by the American Association for the Advancement of Science, 1200 New York Avenue NW, Washington, DC 20005. 

tide groups include parts of the adenine ring and the phosphate-distal face of the ribose moiety. These surface-exposed groups are identical in both AMP- and ATP-bound structures, suggesting that the nucleotide-binding face of the AMPK regulatory trimer is unlikely to function as the site of activation modulated by adenylate binding. The primary differences between AMP- and ATP-bound forms of the heterotrimer lie within the phosphate tunnel. One substantial difference between the ATP and AMP complexes is in the surface electrostatic potentials at the distal exit of the phosphate tunnel, the putative kinase-interaction face (Fig. 2, D to G). This suggests the possibility that the different effects of these ligands might arise from the charge difference between the mono- and triphosphate groups of AMP and ATP.

Prior studies have identified a number of mutations within the regulatory heterotrimer that lead to impaired function of AMPK, primarily in the γ subunit (*1*). These mutations include an insertion in helix E at position γ91 (*32*), and a point mutation at γS247 (N488I in human γ2) (*33*), which is found within the dimer-of-trimers interface region. However, the large majority of functionally important mutations, which include changes to residues γR290 (human γ2 R531) (*34*), γR141 (human γ2 H383) (*32*), γV56 (human γ2 R302) (*35*), and γT162 (human γ2 T400N) (*33*), are all found lining the interior surface of the phosphate tunnel (Fig. 3, A and B). Residues γR290 and γR141 coordinate nucleotide phosphates; however, the other mutations, relative to the bound nucleotide phosphate groups, are positioned further toward the protein surface opposite to the nucleotide binding face. This face of the molecule, where α, β, and γ subunits meet, may constitute a region for KD interaction, and we thus refer to it as the putative kinase domain interaction face (Figs. 1B and 3).

The phosphate tunnel traverses the γ subunit, defining a large void that is capped on the KD-binding face by a polar loop from the β subunit. We refer to this loop, which includes residues 244 to 255, as the β flap. The region of the β flap that covers the phosphate tunnel includes only polar and charged residues and makes no contacts to the hydrophobic core, suggesting the possibility for structural rearrangement. The β flap appears to be highly mobile (average *B* factors of 84.3 $Å^2$ in the four independent β subunits, as compared with an overall average *B* factor of 51.6 $Å^2$ for all protein atoms) and adopts slightly different conformations in the four independent copies of the structures presented here. The majority of γ-subunit mutations that affect AMPK activation are positioned within the phosphate tunnel, between the terminal phosphate of bound AXP and the β flap. Because the difference between the inhibitory (ATP) and activating (AMP) ligands is in the number of phosphates placed within the tunnel and because mutants that affect kinase activation also lie within this tunnel, it appears likely that this represents a critical regulatory region.

We have presented crystal structures that define the core heterotrimeric architecture for AMPKs. The *S. pombe* AMPK binds either AMP or ATP at a single site, suggesting that activating ligands such as AMP are likely to function by displacing the inhibitory ligand ATP. Nonetheless, possible binding of additional regulatory nucleotides in the context of nucleotide mixtures or the holoenzyme complex cannot be excluded. Although a detailed understanding of the mechanism of AMPK regulation will require structures of the holoenzyme, the structures presented here should provide an entry point for the rational design of AMPK-directed therapeutics.

### References and Notes


1. B. B. Kahn, T. Alquier, D. Carling, D. G. Hardie, *Cell Metab.* **1**, 15 (2005).
2. D. G. Hardie, *Endocrinology* **144**, 5179 (2003).
3. B. E. Kemp *et al.*, *Biochem. Soc. Trans.* **31**, 162 (2003).
4. T. Leff, *Biochem. Soc. Trans.* **31**, 224 (2003).
5. D. G. Hardie, S. A. Hawley, J. W. Scott, *J. Physiol.* **574**, 7 (2006).
6. S. B. Jorgensen, E. A. Richter, J. F. Wojtaszewski, *J. Physiol.* **574**, 17 (2006).
7. N. Musi, H. Yu, L. J. Goodyear, *Biochem. Soc. Trans.* **31**, 191 (2003).
8. Y. Minokoshi *et al.*, *Nature* **415**, 339 (2002).
9. T. Yamauchi *et al.*, *Nat. Med.* **8**, 1288 (2002).
10. R. R. Banerjee *et al.*, *Science* **303**, 1195 (2004).
11. V. Lumbreras, M. M. Alba, T. Kleinow, C. Koncz, M. Pages, *EMBO Rep.* **2**, 55 (2001).
12. O. Vincent, R. Townley, S. Kuchin, M. Carlson, *Genes Dev.* **15**, 1104 (2001).
13. S. M. Warden *et al.*, *Biochem. J.* **354**, 275 (2001).
14. G. Polekhina *et al.*, *Structure* **13**, 1453 (2005).
15. J. Adams *et al.*, *Protein Sci.* **13**, 155 (2004).
16. J. Scott *et al.*, *J. Clin. Investig.* **113**, 274 (2004).
17. T. Daniel, D. Carling, *J. Biol. Chem.* **277**, 51017 (2002).
18. S. Meyer, R. Dutzler, *Structure* **14**, 299 (2006).
19. M. D. Miller *et al.*, *Proteins* **57**, 213 (2004).
20. R. Zhang *et al.*, *Biochemistry* **38**, 4691 (1999).
21. S. Meyer, S. Savaresi, I. C. Forster, R. Dutzler, *Nat. Struct. Mol. Biol.* **14**, 60 (2007).
22. T. J. Iseli *et al.*, *J. Biol. Chem.* **280**, 13395 (2005).
23. V. Nayak *et al.*, *Structure* **14**, 477 (2006).
24. M. J. Rudolph, G. A. Amodeo, Y. Bai, L. Tong, *Biochem. Biophys. Res. Commun.* **337**, 1224 (2005).
25. W. A. Hendrickson, J. R. Horton, D. M. LeMaster, *EMBO J.* **9**, 1665 (1990).
26. Single-letter abbreviations for the amino acid residues are as follows: A, Ala; C, Cys; D, Asp; E, Glu; F, Phe; G, Gly; H, His; I, Ile; K, Lys; L, Leu; M, Met; N, Asn; P, Pro; Q, Gln; R, Arg; S, Ser; T, Thr; V, Val; W, Trp; and Y, Tyr.
27. N. Tochio *et al.*, *Protein Sci.* **15**, 2534 (2006).
28. K. A. Wong, H. F. Lodish, *J. Biol. Chem.* **281**, 36434 (2006).
29. X. Zhang *et al.*, *Mol. Cell* **6**, 1473 (2000).
30. W. A. Wilson, S. A. Hawley, D. G. Hardie, *Curr. Biol.* **6**, 1426 (1996).
31. A. Woods *et al.*, *J. Biol. Chem.* **269**, 19509 (1994).
32. E. Blair *et al.*, *Hum. Mol. Genet.* **10**, 1215 (2001).
33. M. Arad *et al.*, *J. Clin. Investig.* **109**, 357 (2002).
34. M. H. Gollob *et al.*, *Circulation* **104**, 3030 (2001).
35. M. H. Gollob *et al.*, *New Engl. J. Med.* **344**, 1823 (2001).

36. Coordinates have been deposited in the Protein Data Bank (accession number for AMP complex is 2OOX; for ATP complex, 2OOY). Crystallographic data were acquired at the New York Structural Biology Center beamline X4A of the National Synchrotron Light Source, Brookhaven National Laboratory. We thank T. Burke and G. Ahlsen for help in biochemical experiments; X. Jin and C. Ciatto for crystallographic help; H. Mu for technical assistance; B. Chait, M. Cadene, and M. Gawinowicz for advice on mass spectrometry analyses; M. Gawinowicz for help in performing them; W. A. Hendrickson and P. D. Kwong for critique of the manuscript; and the reviewers for excellent suggestions. This work was supported in part by a National Institute of Diabetes and Digestive and Kidney Diseases grant and a Jules and Doris Stein Research to Prevent Blindness Foundation professorship award to L.S.

### Supporting Online Material

www.sciencemag.org/cgi/content/full/1137503/DC1
SOM Text
Figs. S1 to S8
Table S1

13 November 2006; accepted 29 January 2007
Published online 8 February 2007;
10.1126/science.1137503
Include this information when citing this paper.

# Structure of Nup58/45 Suggests Flexible Nuclear Pore Diameter by Intermolecular Sliding

**Ivo Melčák, André Hoelz,* Günter Blobel***

**The nucleoporins Nup58 and Nup45 are part of the central transport channel of the nuclear pore complex, which is thought to have a flexible diameter. In the crystal structure of an α-helical region of mammalian Nup58/45, we identified distinct tetramers, each consisting of two antiparallel hairpin dimers. The intradimeric interface is hydrophobic, whereas dimer-dimer association occurs through large hydrophilic residues. These residues are laterally displaced in various tetramer conformations, which suggests an intermolecular sliding by 11 angstroms. We propose that circumferential sliding plays a role in adjusting the diameter of the central transport channel.**

The nuclear pore complex (NPC) mediates the selective exchange of macromolecules between the nucleus and cytoplasm. The NPC is a ringlike structure with an eight-fold symmetry. A central channel is embraced by rings and spokes that are attached to the pore membrane domain of the nuclear envelope (*1*, *2*). Composed of a set of proteins termed nucleoporins (nups), the NPC is one of the largest supramolecular assemblies in the eukaryotic cell (~120 megadaltons in vertebrates) (*3*). About 30 different nups are assembled into multiprotein subcomplexes that serve

Laboratory of Cell Biology, Howard Hughes Medical Institute, The Rockefeller University, 1230 York Avenue, New York, NY 10021, USA.

*To whom correspondence should be addressed. E-mail: hoelza@rockefeller.edu (A.H.), blobel@rockefeller.edu (G.B.)

as the "building blocks" of the NPC (*4*, *5*). Modeling studies have suggested that most nups are constructed from one or two of a small number of structural domains: coiled-coils, α-helical solenoids, β propellers, and natively unfolded segments containing phenylalanine-glycine repeats (FG repeats) (*6*). Current translocation models (*5*, *7*–*9*) are based on the transient, low-affinity binding of cargo-loaded transport factors to FG repeats (*10*–*12*). Large-scale structural rearrangements that occur in response to transport include the constriction and dilation of the central channel, as well as structural alterations of the peripheral assemblies of the NPC (*2*, *13*–*16*). However, at present, the molecular details of the structural changes of the NPC are unknown.

The central channel of the NPC is lined by the Nup62 complex, which consists of Nup62, Nup58, Nup54, and Nup45 (*17*). The constituents of the Nup62 complex display a similar domain organization, in which a ~200-residue α-helical region is flanked by FG repeats (Fig. 1A) (*18*). Of these two distinct structural elements, the α-helical regions are likely to form the perimeter of the channel, whereas the flanking, tentacle-like FG repeats sample the space around the channel, entropically occluding it.

The α-helical regions of all four nups have been predicted to form coiled-coil domains that consist of subdomains separated by short connecting segments (*18*). Nup58 and Nup45 are alternatively spliced forms that differ only in their unstructured region (*19*). The yeast homologs are essential for cell viability (*20*–*22*) and for the formation of a functional "minimal" NPC (*23*).

We assembled a *Rattus norvegicus* Nup62 complex that contains the predicted structured regions of Nup62 (residues 322 to 525), Nup54 (residues 115 to 510), and Nup58 (residues 239 to 415). Through monitoring the formation and stability of complexes, a series of N- and C-terminal deletion constructs was designed. We identified a stable Nup62 complex core that is composed of residues 322 to 525 of Nup62, residues 346 to 494 of Nup54, and residues 327 to 415 of Nup58 (Fig. 1, A and B). The minimal core domains of Nup58 and Nup45 are identical, and therefore, we refer to Nup58 and Nup45 as Nup58/45, using the residue numbering of Nup58 in the text below.

Reconstituted Nup62 complexes form concentration-dependent dynamic assemblies, as judged by size-exclusion chromatography (Fig. 1C). In addition, we analyzed the behavior of a Nup58/45 fragment containing residues 327 to 399 (fig. S1). As do the Nup62 complexes, the Nup58/45 fragment exhibited substantial concentration-dependent mobility, again indicating a dynamic, dimer-tetramer equilibrium in solution. At low salt concentrations, Nup58/45 forms a stable tetrameric assembly, which suggests that the association is governed by electrostatic interactions (fig. S1).

From the purified Nup62 core complex, only the Nup58/45 core domain, composed of residues 327 to 415, crystallized, whereas Nup62, Nup54, and excess Nup58/45 remained intact in the drop solution (fig. S2). Two independent crystallization conditions yielded two Nup58/45 crystal forms, one belonging to the tetragonal space group $P4_322$ and the other to the orthorhombic space group $C222_1$. The structures of both crystal forms were solved by single-wavelength anomalous dispersion (SAD), using osmium-derivatized crystals. The final model was refined to a 2.85 Å resolution with an $R_{work}$ of 25.0% and an $R_{free}$ of 28.8% and contains residues 327 to 411. No electron density was observed for the final four residues that are presumed to be disordered and therefore have been omitted from the final model (table S1).

Nup58/45 tetramers in the two independent crystal forms exhibit entirely different crystal packing arrangements. The asymmetric units of the tetragonal and orthorhombic crystals contain 4 and 18 Nup58/45 protomers, respectively. In the packing of both crystals, the Nup58/45 tetramers result from the dimerization of identical dimers. In each of the two crystal forms, the tetrameric Nup58/45 assemblies are topologically identical, but display distinct structural differences. As the overall findings are similar, we will focus our discussion on the structural information obtained from the tetragonal crystal form.

The Nup58/45 protomer folds into an antiparallel hairpin structure, in which two α helices (the N and the C helix) are connected by a short loop (Fig. 2A). The C helix protrudes from the hairpin structure and exposes three terminal helical turns. The four protomers in the asymmetric unit of the tetragonal crystals are similar, and the topologically equivalent Cα carbons superimpose with a root-mean-square deviation of ~0.4 Å. Furthermore, the protomers dimerize in an antiparallel arrangement, in which the N and C helices of one protomer pack against the N and C helices of the second protomer, forming a four-helix bundle with an interprotomer angle of ~156° (Fig. 2A). The two protomers in the dimer are primarily held together by numerous van der Waals contacts (fig. S3), burying ~2,550 $Å^2$ of surface area. The comparison of the average-temperature B-factors of the entire model (~43 $Å^2$) with the buried dimerization interface residues (~34 $Å^2$) suggests a rigid and well-defined dimer interface. The overall dimensions of the dimer are about 82 by 24 by 21 Å. Except for surface residues, the dimer is symmetric with a pseudo–two-fold axis running through the dimerization interface.

The two identified tetrameric assemblies in both crystal forms consist of two dimers that interact with each other in a "head-to-head" orientation with their N helices. Therefore, the resulting tetramerization interface is composed exclusively by the four N helices that form two antiparallel, intertwined pairs (Fig. 2B). The two tetramers (conformer 1 and 2) of the tetragonal crystal form have two-fold rotational symmetry, and the two-fold symmetry axis of each tetramer coincides with a crystallographic two-fold axis. However, although the crystallographic two-fold axis runs perpendicular to the long axis of the tetramerization interface in one tetramer, it runs parallel to the long axis in the other (Fig. 2B). The crystallographic consequence is that two of the four protomers in each tetramer are identical. The two conformers differ by an ~6 Å lateral displacement of their dimer subunits along the long axis of the tetramerization interface (Fig. 2C). We identified two similar, structurally distinct tetrameric assemblies in the orthorhombic crystal form (conformer 3 and 4), which exhibits an entirely different crystal packing arrangement (fig. S4). The conformation of these tetramers does not appear to be dominated by the crystal packing, as the crystal contains seven structurally independent tetrameric assemblies that give rise to two conformations. All seven tetramers contain a two-fold

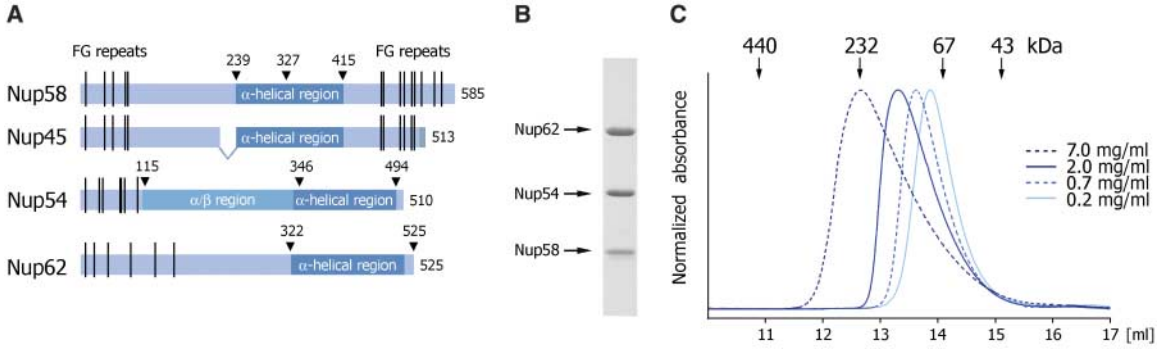


**Fig. 1.** Organization and dynamic behavior of the Nup62 complex. (**A**) Domain structures of Nup58, Nup45, Nup54, and Nup62. The α-helical regions (dark blue), unstructured regions (light blue), FG repeats (black lines), and the numbering of the Nup62 complex fragments are indicated. (**B**) Coomassie-stained SDS–polyacrylamide gel showing results of electrophoresis of the purified Nup62 core complex. (**C**) Gel filtration profiles of the minimal Nup62 complex at the indicated protein concentrations. The elution positions for molecular mass standards are shown. All profiles were obtained in a buffer containing 150 mM NaCl.

axis, which, as do the tetramers in the tetragonal crystal form, run either parallel (three tetramers, conformer 3) or perpendicular (four tetramers, conformer 4) to the long axis of the dimer-dimer interface. However, in contrast to the tetragonal crystal form, only one of the seven tetrameric assemblies is generated by a crystallographic two-fold axis (conformer 3). Thus, the observed tetramerization plasticity is likely an important functional feature of the oligomerization of Nup58/45. Furthermore, the dimer-tetramer dynamics observed in solution likely result from the reversible association of Nup58/45 dimers.

In contrast to the dimerization interface, which is almost entirely hydrophobic, the interactions between the two dimers are solely electrostatic, which explains the salt concentration–dependent, dynamic behavior of Nup58/45 in solution. The tetramerization interface is formed by an extensive side-chain hydrogen bond network that ties the N helices of the four protomers together (Fig. 3). In this tetramerization interface, most of the interactions occur within each pair of aligned, antiparallel N helices, involving primarily the side chains of six residues ($Arg^{333}$, $Gln^{344}$, $Arg^{347}$, $Gln^{348}$, $Glu^{351}$, and $Asn^{355}$) of each protomer. Together, these residues form a continuous electrostatic surface, in which alternating positively and negatively charged side chains are distributed in the center of the interface. The majority of the interactions are mediated by direct intermolecular contacts, although some residues make hydrogen bonds through water molecules trapped at the protein-protein interface. The tetragonal crystals contain two tetrameric Nup58/45 conformers that together contain four unique pairs of N helices. By superposition of all four pairs of N helices, we can discern four different configuration states (states I to IV) that exhibit a maximum lateral displacement of ~11 Å (Figs. 2C and 3). Furthermore, the superposition reveals that the lateral displacement between the two asymmetric tetrameric Nup58/45 conformers results from alternative hydrogen-bond networks, in which each side chain of the same set of interface residues has the propensity to switch interaction partners. For example, the side chain of $Asn^{355}$ engages four different residues in the two tetramers and forms hydrogen bonds with $Gln^{344}$, $Arg^{347}$, $Gln^{348}$, or $Glu^{351}$ (Fig. 3). Overall, the Nup58/45 core domain is highly conserved in vertebrates (figs. S5 and S6). The residues of the Nup58/45 that are crucially involved in the formation of the dimer-dimer interface are invariant across vertebrates, underlining the significance of the Nup58/45 homo-tetramer.

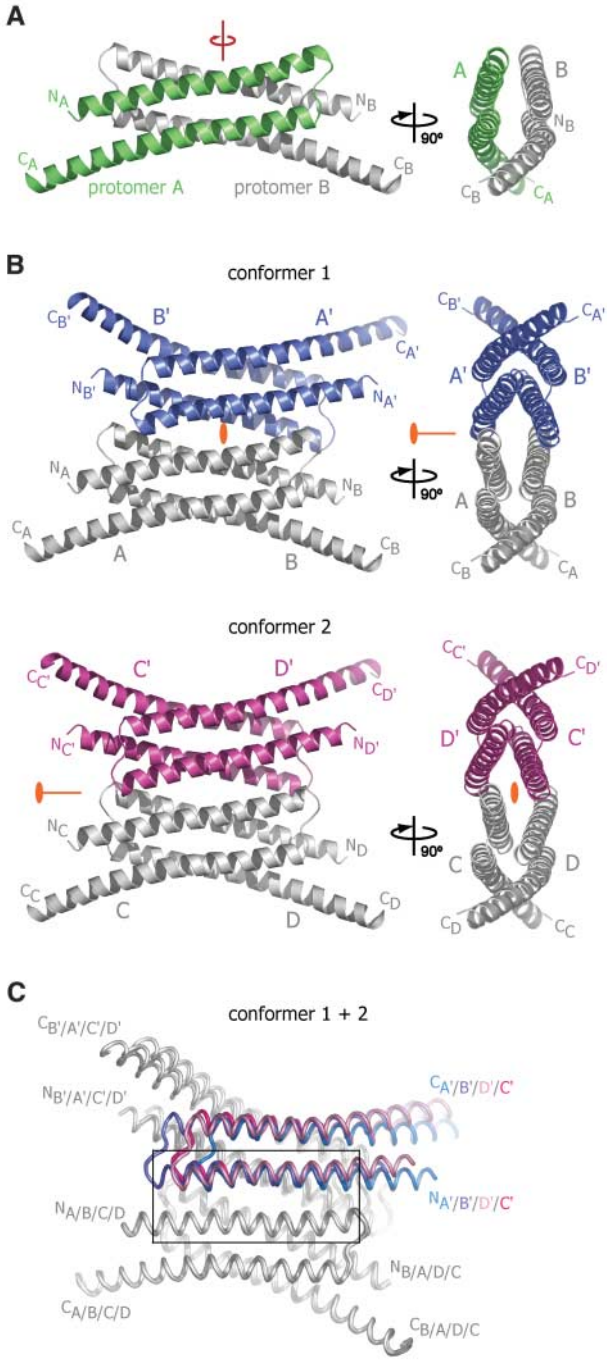


**Fig. 2.** Structures of tetrameric Nup58/45 assemblies from the tetragonal crystal form. (**A**) Ribbon representation of a Nup58/45 dimer, showing protomer A in green and protomer B in gray; (right) a 90° rotated view. A pseudo–two-fold axis (red) is indicated. (**B**) Ribbon representations of the two tetrameric conformers, indicating the location of the crystallographic two-fold axes (orange), which run differently through the two tetramers. (Right) A 90° rotated view. The different coloring of dimers (blue, conformer 1; purple, conformer 2) illustrates the alternative tetrameric configurations of the two conformers. Symmetry-related protomers are indicated. Conformers 1 and 2 are constructed by the protomers A and B, C and D, and their symmetry-related protomers A′ and B′ and C′ and D′, respectively. (**C**) Superposition of the two tetrameric Nup58/45 conformers. The unique protomers of the two tetrameric assemblies are superimposed onto protomer A of conformer 1 to highlight the lateral shift between the different conformers. For clarity, only one protomer of each superposition is colored. The N and C termini are labeled according to (B). The inset is expanded in Fig. 3.

The identification of multiple interaction states in which rigid Nup58/45 dimers are sequentially shifted along the dimer-dimer interface for a distance of ~11 Å suggests an intermolecular sliding mechanism. In general, sliding requires a series of energetically equivalent states along a sliding pathway with low transition energy barriers (*24*). Our sliding hypothesis is strengthened by the finding that the Nup58/45 core domain forms a salt concentration–dependent, dynamic dimer-tetramer equilibrium in solution; this implies that Nup58/45 dimers loosely associate and are indeed capable of freely rearranging into distinct tetrameric conformations. Each of the four states portrays a snapshot of the structural alterations that occur when two Nup58/45 dimers slide against each other on an ~11 Å sliding pathway (Figs. 2C and 3, and movies S1 to S3).

The rearrangement of the dimer-dimer interaction surface that results in the formation of alternative hydrogen-bond networks is enabled by an adaptable electrostatic surface with two major structural features: (i) The interaction surface is constructed by a group of residues that are arranged in a checkerboard-like distribution and that are capable of switching interaction partners by acting alternatively as either hydrogen-bond donors or acceptors, or as both. For example, $Asn^{355}$ alternates its roles in electrostatic interactions with $Gln^{344}$, $Arg^{347}$, $Gln^{348}$, and $Glu^{351}$; (ii) the plasticity of the interaction surface is supported by the relatively high flexibility of long side chains. In contrast to short side chains, long side chains are capable of sampling a substantially larger volume for interaction partners, as illustrated by the alternate conformations of the side chains of $Arg^{333}$ and $Gln^{344}$ in the different tetrameric assemblies.

The central channel of the NPC has the ability to alter its diameter (*2*, *13*, *14*, *16*). The mutual arrangement of subunits within a single Nup58/45

tetramer can be altered by a sliding distance of at least ~11 Å. Nup58 and Nup45 are the most abundant constituents of the NPC (*4*). We propose that circumferential sliding of Nup58/45 in the channel perimeter results in an adjustable diameter in response to transport activity. In such a potentially circular, eight-fold symmetric arrangement of tetrameric Nup58/45 modules in which each can expand by ~11 Å, the diameter of the channel could increase by ~30 Å (Fig. 4, A and B).

In the assembled NPC, Nup58 and Nup45 are intimately associated with Nup54 and Nup62 (*17*, *18*, *25*, *26*). Although the atomic structures for Nup54 and Nup62 have not been determined, they share a similar domain organization and contain conserved, amphipathic α-helical regions that may also permit sliding (figs. S7 to S9). A multiple beltlike arrangement of such "sliding modules" in the channel perimeter along a nucleocytoplasmic axis may facilitate localized changes in channel diameter as cargo passes across (Fig. 4C). The FG repeats are flanking the α-helical regions of the channel nups and function as a restrictive barrier and transport facilitator. It is conceivable that binding of transport factors and substrate to FG repeats is coupled to sliding of the amphipathic helices in the perimeter of the transport channel.

The sliding of such α-helical regions may extend to other nucleoporins, because the export of preribosomal subunits has been shown to depend on the yeast homologs of Nup58 and Nup62 (*27*), as well as the coiled-coil domains of Nup214 and Nup88 (*28*). Our hypothesis of large-scale sliding facilitated by α-helical surfaces to adjust the diameter of a transport channel for the passage of cargo is to our knowledge not found elsewhere and may be limited to macromolecular transport across the NPC.

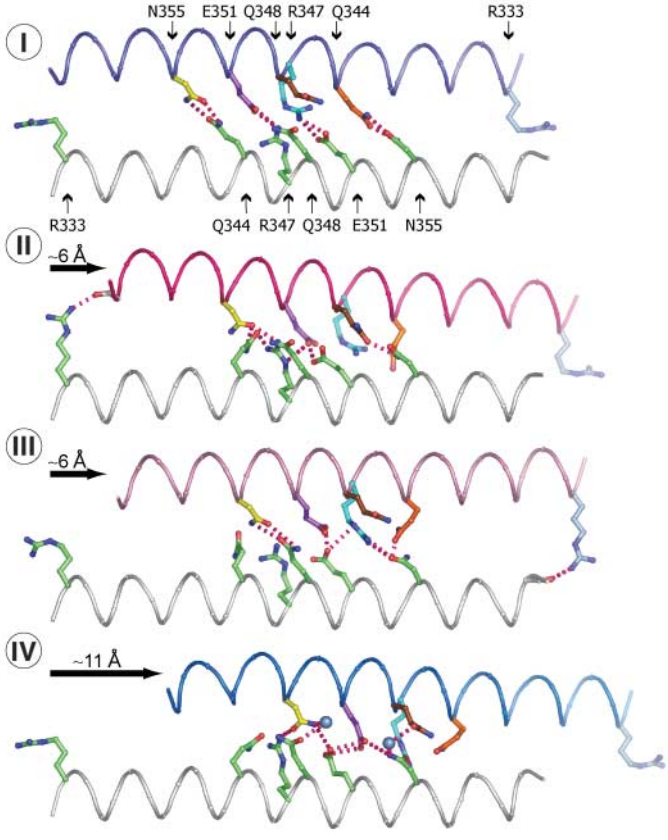


**Fig. 3.** Molecular details of the intermolecular sliding of two Nup58/45 dimers. The direction and the approximate sliding distance are indicated by black arrows. States I and IV are derived from conformer 1; states II and III are derived from conformer 2. The helices are colored and numbered according to Fig. 2, and critical interface residues are labeled and individually colored in all four states according to state I (top). For clarity, only two of the N-helix pairs that generate the tetramerization interface are shown. The electrostatic interactions between two sliding N helices are represented by red dashed lines, and water molecules are visualized as blue spheres.

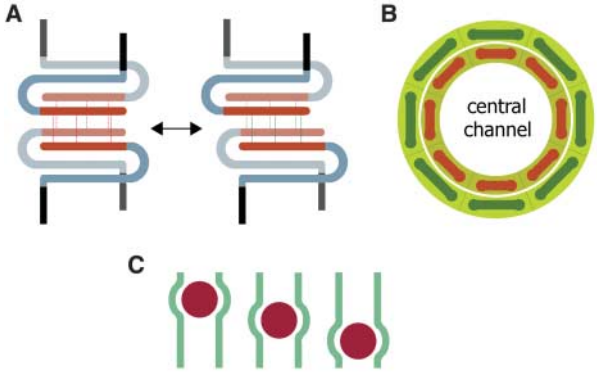


**Fig. 4.** Model of pore dilation by intermolecular sliding of Nup58/45 tetramers. (**A**) Schematic representation of the Nup58/45 sliding module. The four N helices that generate the tetramerization interface (orange), the C helices (light blue), and the C-terminal FG repeats (black) are indicated. The sliding of the Nup58/45 dimer surfaces formed by the N helices is facilitated by an alternative hydrogen bond network (red and green thin lines). Because the C helices with the attached FG repeats are likely to project to the inside of the central channel, the sliding N helices would face in the opposite direction. (**B**) Schematic representation of the central channel shown along the nucleocytoplasmic axis. Eight Nup58/45 tetrameric assemblies are circularly arranged to form a ring (red bars). The sliding of two Nup58/45 dimers against each other results in an overall extension of the Nup58/45 tetramer (green bars) that, in turn, causes the dilation of the central channel of the NPC. (**C**) Localized changes in channel diameter by α-helical sliding in response to transport of cargo (red spheres) across the central channel (green).

## References and Notes


1. D. Stoffler *et al.*, *J. Mol. Biol.* **328**, 119 (2003).
2. M. Beck *et al.*, *Science* **306**, 1387 (2004).
3. R. Reichelt *et al.*, *J. Cell Biol.* **110**, 883 (1990).
4. J. M. Cronshaw, A. N. Krutchinsky, W. Zhang, B. T. Chait, M. J. Matunis, *J. Cell Biol.* **158**, 915 (2002).
5. M. P. Rout *et al.*, *J. Cell Biol.* **148**, 635 (2000).
6. D. Devos *et al.*, *Proc. Natl. Acad. Sci. U.S.A.* **103**, 2172 (2006).
7. I. Ben-Efraim, L. Gerace, *J. Cell Biol.* **152**, 411 (2001).
8. K. Ribbeck, D. Gorlich, *EMBO J.* **20**, 1320 (2001).
9. R. Y. H. Lim *et al.*, *Proc. Natl. Acad. Sci. U.S.A.* **103**, 9512 (2006).
10. R. Bayliss, T. Littlewood, M. Stewart, *Cell* **102**, 99 (2000).
11. S. Fribourg, I. C. Braun, E. Izaurralde, E. Conti, *Mol. Cell* **8**, 645 (2001).
12. T. A. Isgro, K. Schulten, *Structure* **13**, 1869 (2005).
13. C. W. Akey, *Biophys. J.* **58**, 341 (1990).
14. C. W. Akey, D. S. Goldfarb, *J. Cell Biol.* **109**, 971 (1989).
15. E. Kiseleva, M. W. Goldberg, B. Daneholt, T. D. Allen, *J. Mol. Biol.* **260**, 304 (1996).
16. E. Kiseleva, M. W. Goldberg, T. D. Allen, C. W. Akey, *J. Cell Sci.* **111**, 223 (1998).
17. T. Guan *et al.*, *Mol. Biol. Cell* **6**, 1591 (1995).
18. T. Hu, T. Guan, L. Gerace, *J. Cell Biol.* **134**, 589 (1996).
19. T. Hu, L. Gerace, *Gene* **221**, 245 (1998).
20. E. C. Hurt, *EMBO J.* **7**, 4323 (1988).
21. S. R. Wente, M. P. Rout, G. Blobel, *J. Cell Biol.* **119**, 705 (1992).
22. P. Grandi, N. Schlaich, H. Tekotte, E. C. Hurt, *EMBO J.* **14**, 76 (1995).
23. L. A. Strawn, T. Shen, N. Shulga, D. S. Goldfarb, S. Wente, *Nat. Cell Biol.* **6**, 197 (2004).
24. M. Slutsky, L. A. Mirny, *Biophys. J.* **87**, 4021 (2004).
25. D. R. Finlay, E. Meier, P. Bradley, J. Horecka, D. J. Forbes, *J. Cell Biol.* **114**, 169 (1991).
26. C. Macaulay, E. Meier, D. J. Forbes, *J. Biol. Chem.* **270**, 254 (1995).
27. E. Hurt *et al.*, *J. Cell Biol.* **144**, 389 (1999).
28. R. Bernad, D. Engelsma, H. Sanderson, H. Pickersgill, M. Fornerod, *J. Biol. Chem.* **281**, 19378 (2006).


29. We thank Š. Melčáková, M. Müller, and T. Schwartz for help at the initial stages of the project; L. Gerace for the gift of cDNAs; B. Manjasetty (National Synchrotron Light Source) and C. Ralston (Advanced Light Source) for their excellent scientific support and help with x-ray measurements; T. Huber for stimulating discussions; E. Coutavas, M. King, A. Patke, and S. Solmaz for critical reading of the manuscript; and S. Etherton for help with editing of the manuscript. A.H. was supported by a grant from the Leukemia and Lymphoma Society. G.B. is an investigator of the Howard Hughes Medical Institute. The coordinates and structure factors have been deposited in the Protein Data Bank (accession code 2OSZ).


## Supporting Online Material

www.sciencemag.org/cgi/content/full/315/5819/1729/DC1
Materials and Methods
Figs. S1 to S9
Table S1
References
Movies S1 to S3

29 September 2006; accepted 16 February 2007
10.1126/science.1135730